J Mater Sci: Mater Electron (2016) 27:1350–1356
DOI 10.1007/s10854-015-3896-0

Preparation of long persistent phosphor $SrAl_2O_4:Eu^{2+}$, Dy^{3+} and its application in dye-sensitized solar cells

Jinfang Zhang[1] · Jianming Lin[1] · Jihuai Wu[1] · Sheng Zhang[1] · Pei Zhou[1] · Xin Chen[1] · Rui Xu[1]

Received: 16 August 2015 / Accepted: 12 October 2015 / Published online: 26 October 2015

Abstract $SrAl_2O_4:Eu^{2+}$, Dy^{3+} powder has been successfully prepared via a combustion method and then introduced into the titanium dioxide (TiO_2) film photoanode of the dye-sensitized solar cell (DSSC). The influence of the amount of doping on the light-to-electric energy conversion efficiency was discussed. At the concentration 7 wt% of $SrAl_2O_4:Eu^{2+}$, Dy^{3+} (weight ratio of phosphor powder to TiO_2), an overall 20 % improvement was achieved compared to that of the DSSC without $SrAl_2O_4:Eu^{2+}$, Dy^{3+} phosphor doping. The enhancement is mainly due to the presence of the long persistent phosphor doping. It can convert ultraviolet to visible luminescence via down-conversion luminescence. Owing to the emission of long persistent light, the DSSC with $SrAl_2O_4:Eu^{2+}$, Dy^{3+} showed an efficiency of 0.0076 % in the dark after illuminated under a simulated solar light for 1 min. This method represents a novel approach to increase the efficiency of DSSC.

1 Introduction

The supply of non-renewable resources is becoming more serious. Global energy consumption is increasing and is expected to double by the end of 2050. So, the search for alternative renewable energy sources is undoubtedly important [1, 2]. Sunlight is a freely available abundant source of solar energy which can irradiate the Earth's surface with 120,000 TW of solar power [3].

Dye-sensitized solar cell (DSSC) is a photoelectric power generation device, which can convert light photons into electricity effectively. It was firstly reported by Dr. Gratzel's group in 1991 [4]. Since then, the research of the DSSC has become a hot topic owing to its environmentally friendly and low-cost character. A conventional DSSC is assembled by a photoelectrode of dye adsorbed on porous nanocrystalline titanium dioxide (TiO_2), a counter electrode of platinum [5].

The dye-sensitized TiO_2 photoanode plays an important part in the absorbing sunlight, it can load sensitizers and collect and transport electrons. However, it only absorbs visible light in the wavelength range 300–800 nm. The absorption in the ultraviolet spectrum and red region of the visible spectrum is restricted. Thus, in order to improve the harvest of incident light, many new-type dyes have been under observation [6]. An effective way to improve the conversion efficiency is the utilization of a luminescence layer composed of up-conversion (UC) or down-conversion (DC) phosphor materials [7–9]. It can convert ultraviolet or red irradiation into visible light and more solar irradiation will be utilized, the DSSC photocurrent may increase. Recently, Yao et al. [10] applied a DC phosphor layer composed of $ZnO:Eu^{3+}$, Dy^{3+} to DSSC. It can broaden absorption region of solar spectrum in DSSC and enhanced carrier transportation is achieved. Meanwhile, a down convertor $Lu_3Al_5O_{12}:Ce^{3+}$ (LuAG) phosphor was used as a visible light amplifier for DSSC [11]. LuAG particles emitting green light, which are capable of stimulating Ru-dye molecules, enhanced the light-harvesting properties of a DSSC.

So far, the rare earth luminescent material used in DSSC mainly are fluorescent materials, however, the introduction

✉ Jianming Lin
jmlin@hqu.edu.cn

[1] Engineering Research Center of Environment-Friendly Functional Materials of the Ministry of Education, Key Laboratory for Functional Materials of Fujian Higher Education, Institute of Material Physical Chemistry, Huaqiao University, Xiamen 361021, China

of long persistent phosphor in the DSSC is rarely reported. Green emitting $SrAl_2O_4$ co-doped with Eu^{2+}, Dy^{3+} ions has been considered one of the best and long lasting phosphorescent materials [12]. In this paper, $SrAl_2O_4$:Eu^{2+}, Dy^{3+} powder has been synthesized by combustion method and applied in the DSSC. The prepared phosphor powder has the characteristic of DC luminescence and light-to-electric energy conversion efficiency is improved. The research result reveals that the long persistent phosphor $SrAl_2O_4$:Eu^{2+}, Dy^{3+} can be a candidate material to improve the efficiency of DSSC.

2 Experimental

2.1 Materials

Tetrabutyl titanate, absolute ethyl alcohol, glacial acetic acid, polyethylene glycol 20,000, 4-tert-butylpyridine (TBP), nitric acid, OP emulsification agent (Triton X-100), iodine, lithium iodide, urea, boric acid, aluminium nitrate and strontium nitrate were analytic purity supplied by Shanghai Chemical Agent Limited, Shanghai, China. The sensitized dye N-719 [$RuL_2(NCS)_2$, L = 4,4′-dicarboxylate-2,2′-bipyridine] was from SOLARO-NIX SA (Aubonne, Switzerland). Dysprosium oxide and europium oxide were supplied by Shanghai Yuelong Non-Ferrous Metals Limited, Shanghai, China.

2.2 Preparation of $SrAl_2O_4$:Eu^{2+}, Dy^{3+} powder

The $SrAl_2O_4$:Eu^{2+}, Dy^{3+} phosphor powder was synthesized by combustion technique. Amounts of urea were added as reducer and fuel, small quantities of boric acid were used as a flux, metal nitrates were used as oxidizer. Powders were weighted according to the stoichiometry.

The procedure used to prepare the precursor had the following stages. Firstly, Eu_2O_3 (0.088 g) and Dy_2O_3 (0.093 g) were dissolved into concentrated nitric acid (1.4 g/ml) to form nitrate solution. $Al(NO_3)_3{\cdot}9H_2O$ (7.5 g), $Sr(NO_3)_2$ (2.116 g), H_3BO_3 (0.18 g) and $CO(NH_2)_2$ (15 g) were dissolved enough into deionised water to obtain transparent solution, then mixed the two solutions together and stirred at 70 °C for 4 h to make some water evaporate.

After that, the precursor solution was introduced into a muffle furnace maintained at 600 °C. Initially, the solution boiled and underwent dehydration, followed by decomposition with escaping large amounts of gases (oxides of carbon, nitrogen and ammonia) and then spontaneous ignition occurred and underwent smouldering combustion with enormous swelling, producing white foamy and voluminous ash, the whole process was over within less than 5 min, after the product was cooled to room temperature, milled the ash slightly. The $SrAl_2O_4$:Eu^{2+}, Dy^{3+} phosphor was obtained.

2.3 Preparation of $SrAl_2O_4$:Eu^{2+}, Dy^{3+}/TiO_2 photoanode

First, the TiO_2 colloid was prepared as reported in our previous work [13–15]. Then a different amount of $SrAl_2O_4$:Eu^{2+}, Dy^{3+} powders (0, 3, …, 9 wt%) were dispersed in the TiO_2 colloid by stirring and ultrasonic treatment for 30 min respectively. After that, keep the colloid stirring under 105 °C until it becomes thicken and homogeneous. The resulting colloid was deposited on the FTO electrode by a doctor blade coating. The first layer with about 10 μm thickness was coated with pure TiO_2. After drying under an infrared lamp, the TiO_2 film was sintered at 450 °C for 30 min and cooled down to 80 °C. The second layer with about 4 μm thickness was coated with $SrAl_2O_4$:Eu^{2+}, Dy^{3+}/TiO_2 colloid by the same method. Finally, $SrAl_2O_4$:Eu^{2+}, Dy^{3+}/TiO_2 photoanode was obtained. Figure 1 shows a sketch of the structure of the DSSC. For comparison, the DSSC without $SrAl_2O_4$:Eu^{2+}, Dy^{3+} containing layer was assembled.

2.4 Fabrication of the DSSC

The $SrAl_2O_4$:Eu^{2+}, Dy^{3+}/TiO_2 photoelectrode was immersed into the N719 dye-ethanol solution at room temperature in the dark for 24 h. Then a DSSC was assembled by injecting the redox electrolyte [0.1 M I_2, 0.1 M LiI, 0.6 M $N(n\text{-}C_4H_9)_4I$ and 0.5 M TBP in acetonitrile] into interspace between the $SrAl_2O_4$:Eu^{2+}, Dy^{3+}/TiO_2 photoelectrode and a platinum counter electrode. The DSSC based on a pure TiO_2 photoelectrode was prepared using the same method.

2.5 Characterization

Field emission scanning electron microscopy (FESEM, SU8000, Hitachi, Japan) was used to study the phosphor morphology. Energy Dispersive Spectrometer (EDS, INCA Energy, OXFORD, UK) was performed to analyze the chemical elements. The crystal structure of the powder was identified by an X-ray diffractometer (XRD, Bruker D8 Advance, Germany) using Cu Kα radiation ($\lambda = 1.5405$ Å). The 2 θ angle of the XRD spectra was recorded at a scanning rate of 5° min^{-1}. The photovoltaic testing of the DSSCs was performed by measuring the photocurrent density-cell potential curves under a simulated solar light coming from a 3A solar simulator (94043A, Newport Corporation, America) equipped with a Xe lamp (450 W) and an AM1.5G filter. The impedance measurements were carried out in dark atmosphere and studied on CHI660E (Shanghai Chenhua Device Company, China). The excitation and emission spectra were obtained from a fluorescence spectrometer (Lumina, Thermo Scientific, America).

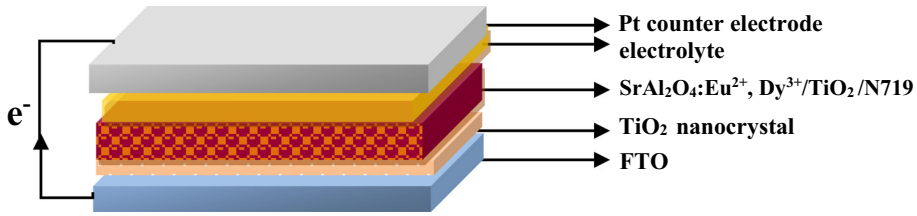

Fig. 1 Schematic representation of the DSSC

The decay curve was recorded using a fluorescence spectrophotometer (FLS980, Edinburgh, UK) fitted with a xenon lamp after the sample was sufficiently excited for about 15 min. UV–Vis diffuse reflection tests were performed with an UV/Vis–NIR spectrometer (Lambda 950, PerkinElmer, America).

3 Results and discussions

3.1 Morphology and structure characterizations

Field emission scanning electron microscopy (FESEM) measurements were carried out to observe the morphology and size of the sample. Figure 2a shows the FESEM image of the prepared strontium aluminate crystal. Figure 2b shows the surface morphology of the $SrAl_2O_4:Eu^{2+}$, Dy^{3+}/TiO_2 photoelectrode.

From Fig. 2a, we can see there are many cracks, voids and pores formed on the surface of the foams due to the escaping gases during combustion reaction. The large amount of escaping gases can dissipate heat so as to prevent the material from sintering and contribute to the formation of nanocrystalline phase. The phosphor particles are irregular. The obvious phenomenon of agglomeration suggests the crystal activity of the generated phosphor powder is very high. Figure 2b indicates the successful doping of $SrAl_2O_4:Eu^{2+}$, Dy^3. Energy-dispersive X-ray Spectroscopy (EDS) was carried to analyse the composition of the $SrAl_2O_4:Eu^{2+}$, Dy^3/TiO_2 photoelectrode, as exhibited in Fig. 2c, which shows that as-synthesized sample composed of Sr, Al, O, Ti, Dy and Eu Elements and no other spurious impurity elements were detected. The results further confirm the existence of TiO_2 and $SrAl_2O_4:Eu^{2+}$, Dy^3.

Figure 3 displays a typical X-ray diffraction pattern of the resultant TiO_2, $SrAl_2O_4:Eu^{2+}$, Dy^{3+} and $SrAl_2O_4:Eu^{2+}$, Dy^3/TiO_2 respectively. The pure monoclinic phase diffraction peaks of $SrAl_2O_4$ are predominant in the XRD pattern. Each diffraction peak in the pattern is similar with the standard pattern of $SrAl_2O_4$ JCPDS data (No. 34-0379). It means $SrAl_2O_4:Eu^{2+}$, Dy^{3+} phosphor belongs to a P21

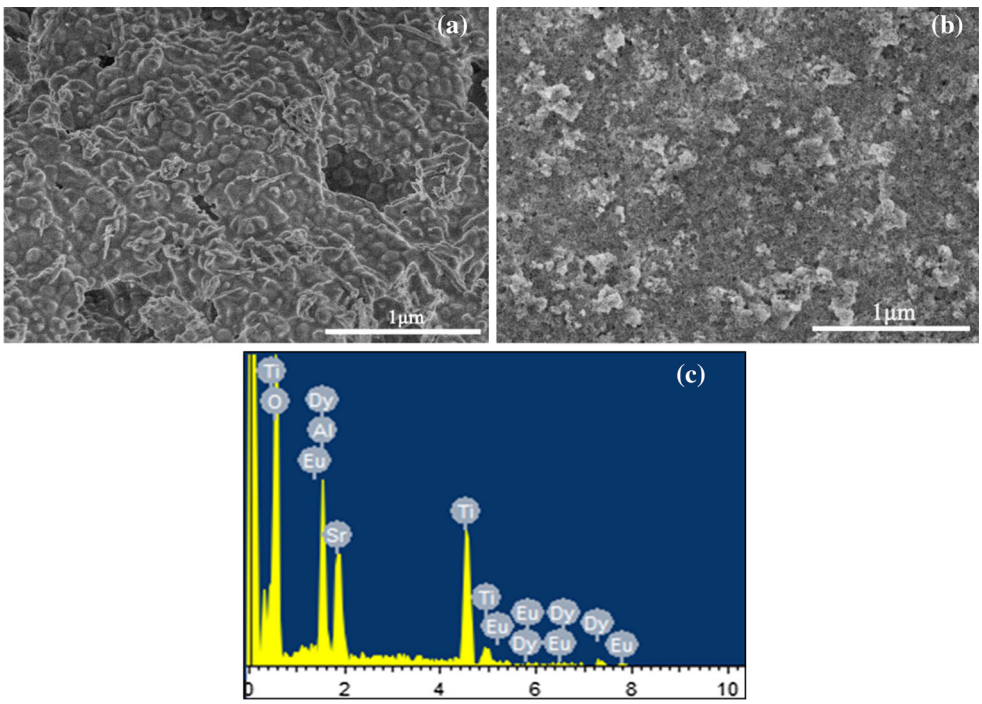

Fig. 2 FESEM pattern of **a** $SrAl_2O_4:Eu^{2+}$, Dy^{3+} powder and **b** $SrAl_2O_4:Eu^{2+}$, Dy^{3+}/TiO_2 photoelectrode. **c** EDS pattern of $SrAl_2O_4:Eu^{2+}$, Dy^3/TiO_2 photoelectrode

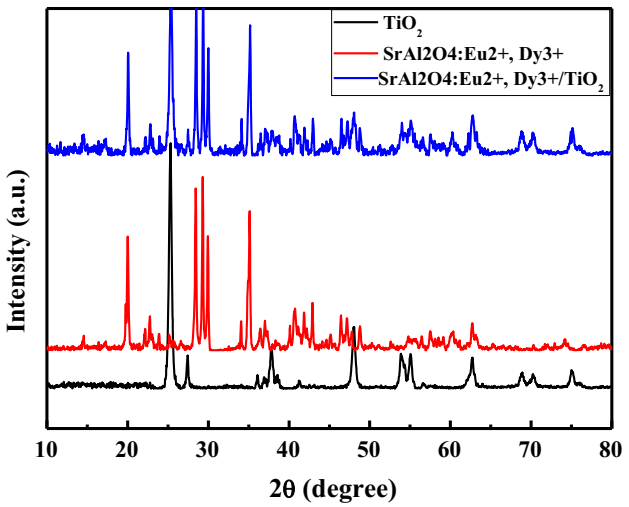

Fig. 3 XRD patterns of TiO_2, $SrAl_2O_4$:Eu^{2+}, Dy^{3+} and $SrAl_2O_4$:Eu^{2+}, Dy^3/TiO_2

space group and a monoclinic system (a = 8.442 Å, b = 8.822 Å, c = 5.160 Å, β = 93.415°). The result indicates the crystalline phase of $SrAl_2O_4$ when doped with Eu^{2+} and Dy^{3+} rare earth ions. The small amount of Eu^{2+} and Dy^{3+} doped ions enter the host lattice and replace Sr^{2+} ion partly, they have almost no effect on the $SrAl_2O_4$ phase composition [16]. Besides, other obvious diffraction peaks can't be found in the XRD pattern, proving the resultant material doesn't contains other crystalline phases. The phase diffraction peaks of pure TiO_2 are also presented in the XRD pattern. It is clear to see that the diffraction peaks of TiO_2 located at 25.3°, 37.2°, 48.0°, 53.7°, 55.0°, 63.0°, 69.0°, 70.2° and 75.0° can be respectively indexed to the (101), (004), (112), (200), (105), (211), (204), (116), (220), and (215) crystal planes of anatase TiO_2 (JCPDS card 21-1272). Compared with the pure TiO_2 and single phosphor powder, all the major diffraction peaks of TiO_2 and $SrAl_2O_4$ can be found and no extra peak was detected in the XRD pattern of $SrAl_2O_4$:Eu^{2+}, Dy^3/TiO_2, which suggests that the $SrAl_2O_4$:Eu^{2+}, Dy^{3+} particles have combined with the TiO_2 colloid.

3.2 The properties of $SrAl_2O_4$:Eu^{2+}, Dy^{3+} powder

Figure 4a shows the excitation and emission spectra spectrums of $SrAl_2O_4$:Eu^{2+}, Dy^{3+}. It shows a broad band and at maximum excitation peak the corresponding excitation wavelength of is 370 nm which is assigned to the characteristic $4f^7 \rightarrow 4f^65d^1$ transition of the Eu^{2+} ion. The emission spectra at room temperature of $SrAl_2O_4$:Eu^{2+}, Dy^{3+} was shown in the Fig. 4b at excitation wavelength of 370 nm, it yields high bright green luminescence (λ_{max} = 520 nm) with only one broad band which is due to the typical $4f^65d^1 \rightarrow 4f^7$ transition of luminescent center Eu^{2+} ion [17]. Dy^{3+} ion is an auxiliary active ion and work as a hole trap which generates the trap energy level in the original matrix. It is the hole trapped–transported–de-trapped process that results in the properties of long afterglow of $SrAl_2O_4$:Eu^{2+}, Dy^{3+} phosphor [18]. The luminescence 520 nm is just within the absorption wavelength range of commonly used dye N719. In addition, the ultraviolet irradiation from the sun can be reabsorbed by the dye N719 via the DC luminescence of $SrAl_2O_4$:Eu^{2+}, Dy^{3+} and contributes to the solar light harvest of DSSC. Besides, from the UV–Vis diffuse reflection spectroscopy shown in Fig. 4c, an obvious absorption was exhibited in the 200–400 nm region which improved the light scattering capabilities of the dye, resulting in an improved light harvesting ability.

The decay characteristics of $SrAl_2O_4$:Eu^{2+}, Dy^{3+} phosphor was tested by continuous exciting with 370 nm UV light for about 15 min. The measurements started in the darkness after the excited source was cut off. As we can see in the Fig. 5, the decay processes of $SrAl_2O_4$:Eu^{2+}, Dy^{3+} phosphor contain the rapid-decaying process and the slow-decaying one. The initial intensity of phosphor is very high and then the intensity of the afterglow decreases rapidly and finally formed a stable long persistent emission. As we know, the roles of Eu^{2+} ions are the luminescent centers and Dy^{3+} ions serve as the luminescent centers in aluminate phosphors. The first decay process could be attributed to the short survival time of the electron in Eu^{2+} while the slow decay process results from the deep trap energy center of Dy^{3+}. It can be seen from the afterglow decay curve that the $SrAl_2O_4$:Eu^{2+}, Dy^{3+} phosphor we have prepared exhibited a good afterglow property.

3.3 The photoelectric performance of the DSSC

The photovoltaic parameters including the open-circuit voltage (V_{OC}), short-circuit density (J_{SC}), fill factor (FF) and overall light-to-electrical energy conversion efficiency (η) of these DSSCs under a simulated solar light irradiation of 100 mW cm^{-2} are summarized in Table 1 and the photocurrent-voltage curves of the DSSC with and without $SrAl_2O_4$:Eu^{2+}, Dy^{3+} dopant are showed in Fig. 6. Table 1 shows that J_{SC} and increased with the $SrAl_2O_4$:Eu^{2+}, Dy^{3+} dopant level up to 7 wt%, beyond which J_{SC} decreased. The increase in J_{SC} comes mainly from the introduction of long persistent phosphors, which caused more sunlight to be harvested, thus increasing J_{SC}. After that, the large amounts of phosphors influence the TiO_2 crystal gap, which cause the block of electronic transmission and the decrease of J_{SC} [19, 20]. While FF increased gradually, from 0.662 to 0.729 V.

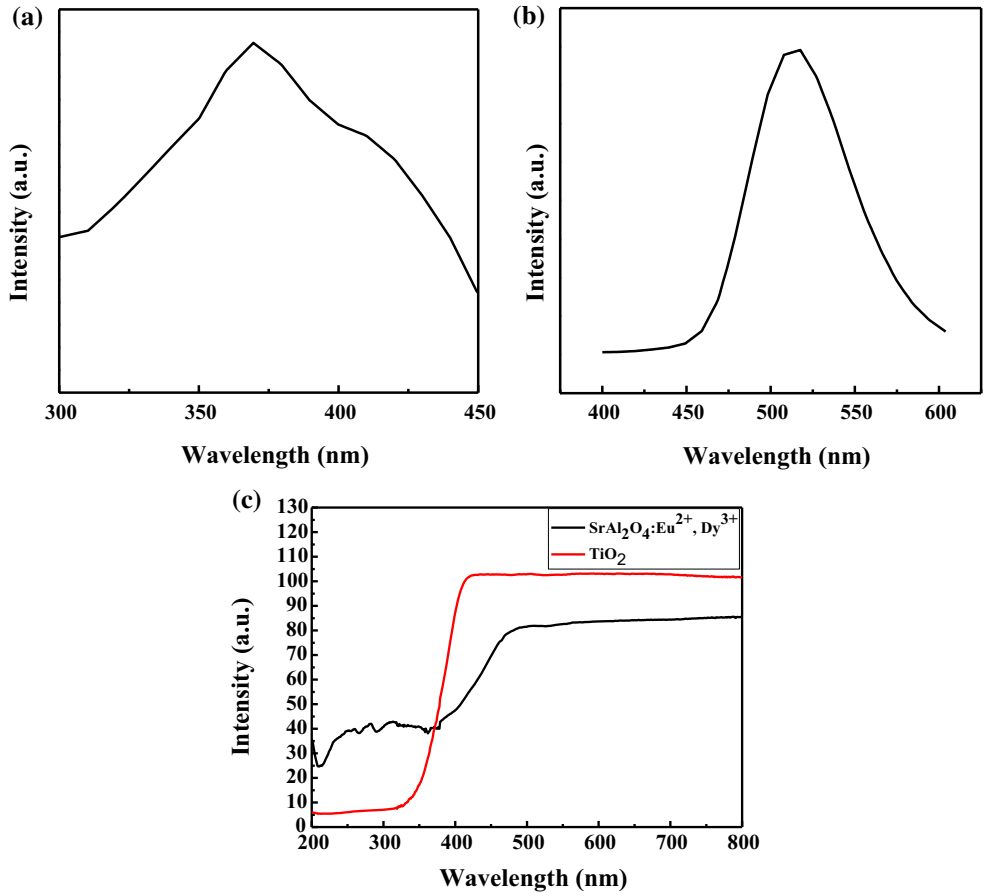

Fig. 4 Excitation spectra spectrum (**a**) and emission spectra spectrum of $SrAl_2O_4:Eu^{2+}$, Dy^{3+} (**b**) UV–Vis-DRS spectra of TiO_2 nanoparticles and $SrAl_2O_4:Eu^{2+}$, Dy^{3+} powder (**c**)

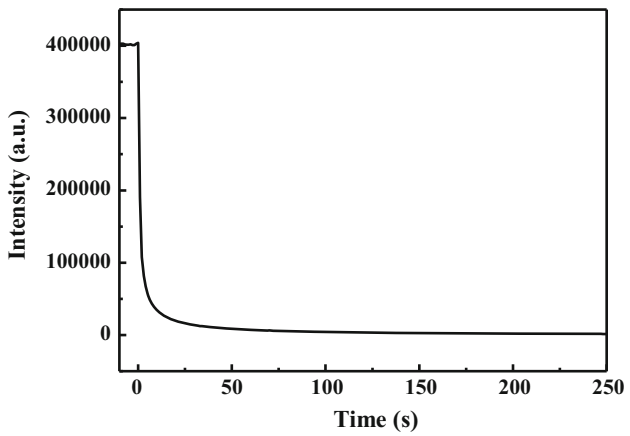

Fig. 5 Afterglow decay curve of $SrAl_2O_4:Eu^{2+}$, Dy^{3+} phosphor after exciting for 15 min

As we can see in Fig. 6, an obvious increasement of the sunlight conversion efficiency for DSSC with $SrAl_2O_4:Eu^{2+}$, Dy^{3+} dopant. The DSSC without dopant displays the photovoltaic parameters: $V_{OC} = 0.797$ V, $J_{SC} = 12.54$ mA cm^{-2}, FF = 0.662 $\eta = 6.62$ %. And DSSC with $SrAl_2O_4:Eu^{2+}$, Dy^{3+} dopant demonstrates enhanced photovoltaic parameters: $V_{OC} = 0.828$ V, $J_{SC} = 13.41$ mA cm^{-2}, FF = 0.715, $\eta = 7.94$ %. The enhancement mainly due to the DC luminescence response of $SrAl_2O_4:Eu^{2+}$, Dy^{3+} which transfers the ultraviolet light to visible light and broadens the absorption spectrum of the DSSC. As a result, more photoinduced electrons can be produced to enhance the photocurrent, increasing the harvested sunlight and efficiency of DSSC was improved.

The DSSC with $SrAl_2O_4:Eu^{2+}$, Dy^{3+} dopant has a unique property compared with the pure TiO_2 electrode for its emission of long persistent light. After the DSSCs were illuminated under a simulated solar light for 1 min, the light source was turned off and the photovoltaic performance of the cells was measured in the dark. Table 2 lists the different data between the cells containing the TiO_2 and $SrAl_2O_4:Eu^{2+}/TiO_2$ electrodes. The efficiency of the DSSC with $SrAl_2O_4:Eu^{2+}$, Dy^{3+} dopant is 0.0076 % in the dark, while the efficiency of the DSSC containing the pure TiO_2 electrode is almost zero. The emission of long persistent light from the long afterglow phosphor makes it possible for a cell works in the dark. This method represents a novel approach to improve the DSSC.

Table 1 Influence of the amount of $SrAl_2O_4:Eu^{2+}$, Dy^{3+} on the photoelectric properties of the DSSC

$SrAl_2O_4:Eu^{2+}$, Dy^{3+} (wt%)	Voc (V)	Jsc (mA cm^{-2})	FF	η (%)
0	0.797	12.54	0.662	6.620
3	0.808	12.73	0.682	7.025
5	0.809	13.01	0.687	7.236
7	0.828	13.41	0.715	7.938
9	0.820	12.77	0.729	7.630

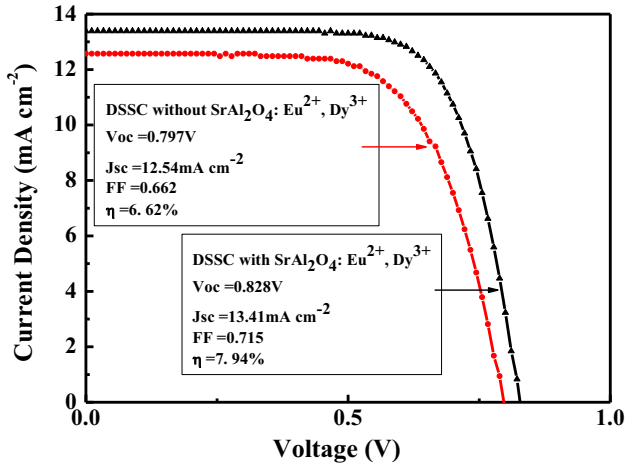

Fig. 6 J–V curves of the DSSC with and without $SrAl_2O_4:Eu^{2+}$, Dy^{3+} dopant (7 wt%)

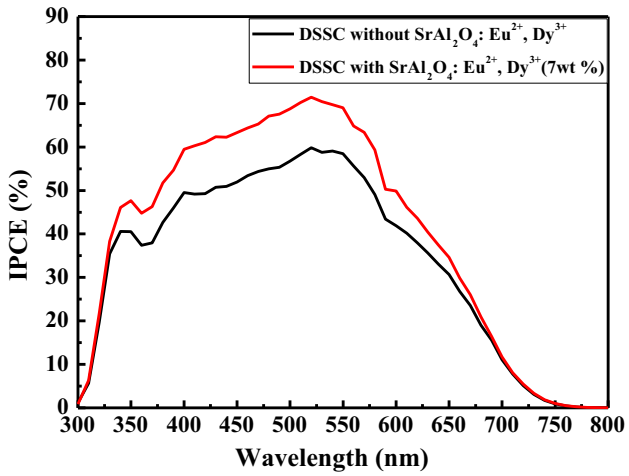

Fig. 7 IPCE spectra of the DSSC without and with $SrAl_2O_4:Eu^{2+}$, Dy^{3+} dopant (7 wt%)

Table 2 Photovoltaic parameters of DSSC without and with $SrAl_2O_4:Eu^{2+}$, Dy^{3+} dopant (7 wt%) in the dark after 100 mW cm^{-2} illumination for 1 min

$SrAl_2O_4:Eu^{2+}$, Dy^{3+} (wt%)	Voc (V)	Jsc (mA cm^{-2})	FF	η (%)
0	0.00016	0.0060	0	0
7	0.461	0.034	0.479	0.0076

As shown in Fig. 7, the photocurrent action (IPCE) spectra show that the absolute IPCE of the cell containing the $SrAl_2O_4:Eu^{2+}$, Dy^{3+} phosphor is higher than the cell containing the pure TiO_2 electrode in both the UV and visible regions, which is in good agreement with the observed higher J_{SC}. The improvement is mainly due to the introduction of $SrAl_2O_4:Eu^{2+}$, Dy^{3+} which could absorb near UV-photons and causes a visible green emission. The excited dye N719 emits green light and excess electrons generate. As a result light harvesting ability within the electrode is enhanced and the quantum efficiency increases.

3.4 The impedance spectra of the DSSC

The charge transfer and recombination behavior in the DSSC were studied by analyzing the EIS spectra in the dark. The EIS spectra in Fig. 8 are characterized by the presence of two semicircles in a Nyquist plot [21, 22]. The smaller semicircle in high frequency region represents the electron ejection at the platinum counter electrode/electrolyte interface (R_1), and the larger one in medial frequency region is related to chemical capacitance of nanostructured TiO_2 and the charge recombination resistance (R_2) which reveals the charger transfer at the TiO_2/Dye/electrolyte interface and transport in the TiO_2 films.

The detailed results are showed in Table 3. R_1 values are similarly obtained for the DSSC with different amount of $SrAl_2O_4:Eu^{2+}$, Dy^{3+} dopant. While R_2 value increased as the doping amount of $SrAl_2O_4:Eu^{2+}$, Dy^{3+} varies from 0 to 7 wt%. The raised value of R_2 is corresponding to the circumstances for charge recombination from the conduction band of the anode materials to the redox I^-/I_3^- couple. The increasing $SrAl_2O_4:Eu^{2+}$, Dy^{3+} in TiO_2 produced some crystal defects, causing electron transport resistance. It means that the charge recombination at the interface of TiO_2/Dye/electrolyte within the DSSC is hindered because of the difficulties in charge transferring in dark condition [23, 24], which is favorable for the improvement of photovoltaic performance.

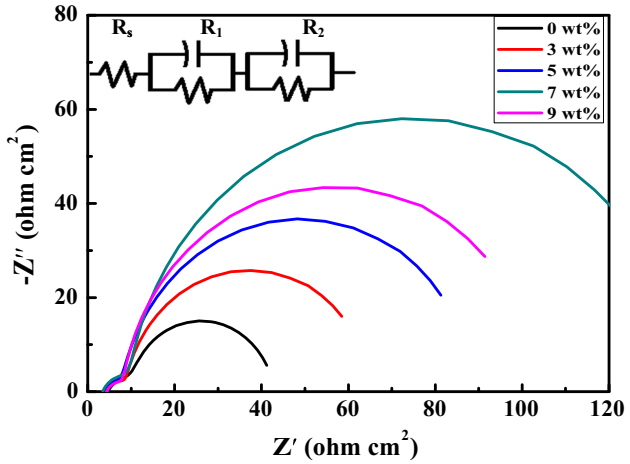

Fig. 8 Nyquist plots of the impedance data of the DSSC with different amount of $SrAl_2O_4:Eu^{2+}$, Dy^{3+} tested in the dark. The *inset* is the equivalent circuit model of the DSSC

Table 3 Fitted data for the EIS measurements of the DSSCs

$SrAl_2O_4:Eu^{2+}$, Dy^{3+} (wt%)	R_1 (Ω cm^{-2})	R_2 (Ω cm^{-2})
0	4.66	38.09
3	5.21	43.71
5	4.58	74.6
7	5.15	117.4
9	4.83	87.77

4 Conclusion

In summary, long persistent phosphor $SrAl_2O_4:Eu^{2+}$, Dy^{3+} was successfully synthesized by combustion method and introduced into a DSSC. As a luminescence medium, $SrAl_2O_4:Eu^{2+}$, Dy^{3+} improved light harvesting via a conversion luminescence process and increased photocurrent. $SrAl_2O_4:Eu^{2+}$, Dy^{3+} elevated the energy level of the oxide film and increased the photovoltage. The solar conversion efficiency for a DSSC with $SrAl_2O_4:Eu^{2+}$, Dy^{3+} doping (7:100) reached 7.938 % under a simulated solar light irradiation of 100 mW cm^{-2}, increased by a factor of 1.32 compared to that of the DSSC without $SrAl_2O_4:Eu^{2+}$, Dy^{3+} phosphor doping. This work demonstrates the feasibility of the long persistent phosphor doping in a DSSC and provides a novel way to enhance the sunlight conversion efficiency for solar cells.

References

1. A.J. Nozik, J. Miller, Chem. Rev. **110**, 6443 (2010)
2. K. Kalyanasundaram, M. Grätzel, J. Mater. Chem. **22**, 24190 (2012)
3. H. Águas, S.K. Ram, A. Araújo, D. Gaspar, A. Vicente, S.A. Filonovich, E. Fortunato, R. Martins, I. Ferreira, Energy Environ. Sci. **4**, 4620 (2011)
4. B. O'Regan, M. Grätzel, Nature **353**, 737 (1991)
5. J. Zhang, X. Li, W. Guo, T. Hreid, J. Hou, H. Su, Z. Yuan, Electrochim. Acta **56**, 3147 (2011)
6. M. Gratzel, Nature **414**, 338 (2001)
7. J. Wu, J. Wang, J. Lin, Z. Lan, Q. Tang, M. Huang, Y. Huang, L. Fan, Q. Li, Z. Tang, Adv. Energy Mater. **2**, 78 (2012)
8. G. Xie, J. Lin, J. Wu, Z. Lan, Q. Li, Y. Xiao, G. Yue, H. Yue, M. Huang, Chin. Sci. Bull. **56**, 96 (2011)
9. J. Zhang, H. Shen, W. Guo, S. Wang, C. Zhu, F. Xue, J. Hou, H. Su, Z. Yuan, J. Power Sources **226**, 47 (2013)
10. N. Yao, J. Huang, K. Fu, S. Liu, E. Dong, Y. Wang, X. Xu, M. Zhu, B. Cao, J. Power Sources **267**, 405 (2014)
11. G.S. Han, Y.H. Song, D.H. Kim, M.-J. Lee, D.G. Lee, S.-H. Han, Y. Kim, M.-K. Jung, D.-H. Yoon, H.S. Jung, RSC Adv. **5**, 24737 (2015)
12. F. Clabau, X. Rocquefelte, S. Jobic, P. Deniard, M.H. Whangbo, A. Garcia, T. Le Mercier, Chem. Mater. **17**, 3904 (2005)
13. J.H. Wu, S.C. Hao, Z. Lan, J.M. Lin, M.L. Huang, Y.F. Huang, L.Q. Fang, S. Yin, T. Sato, Adv. Funct. Mater. **17**, 2645 (2007)
14. J. Wu, S. Hao, Z. Lan, J. Lin, M. Huang, Y. Huang, P. Li, S. Yin, T. Sato, J. Am. Chem. Soc. **130**, 11568 (2008)
15. J.H. Wu, Z. Lan, J.M. Lin, M.L. Huang, S.C. Hao, T. Sato, S. Yin, Adv. Mater. **19**, 4006 (2007)
16. N.M. Son, L.T.T. Vien, L.V.K. Bao, N.N. Trac, J. Phys, Conf. Ser. **187**, 012 (2009)
17. T. Matsuzawa, J. Electrochem. Soc. **143**, 2670 (1996)
18. G. Swati, S. Chawla, S. Mishra, B. Rajesh, N. Vijayan, B. Sivaiah, A. Dhar, D. Haranath, Appl. Surf. Sci. **333**, 178 (2015)
19. K.H. Ko, Y.C. Lee, Y.J. Jung, J. Colloid Interface Sci. **283**, 482 (2005)
20. D. Aberdam, R. Durand, R. Faure, F. Gloaguen, J.L. Hazemann, E. Herrero, A. Kabbabi, O. Ulrich, J. Electroanal. Chem. **398**, 43 (1995)
21. X. Yan, L. Feng, J. Jia, X. Zhou, Y. Lin, J. Mater. Chem. A **1**, 5347 (2013)
22. L.-W. Chong, H.-T. Chien, Y.-L. Lee, J. Power Sources **195**, 5109 (2010)
23. R. Gao, Z. Liang, J. Tian, Q. Zhang, L. Wang, G. Cao, Nano Energy **2**, 40 (2013)
24. Z. Huo, S. Dai, K. Wang, F. Kong, C. Zhang, X. Pan, X. Fang, Sol. Energy Mater. Sol. Cells **91**, 1959 (2007)